W. Cao, S.-L. Chen, F. Zhang, K. Wu, Y. Yang, Y. A. Chang, R. Schmid-Fetzer and W. A. Oates, Calphad, 2009; 33(2): 328-342

PANDAT Software with PanEngine, PanOptimizer and PanPrecipitation for Multi-Component Phase Diagram Calculation and Materials Property Simulation

W. Cao[a], S.-L. Chen[a], F. Zhang[a], K. Wu[a], Y. Yang[a], Y. A. Chang[b]
R. Schmid-Fetzer[c], W. A. Oates[d]

[a] *CompuTherm LLC, 437 S. Yellowstone Dr., Madison WI 53719, U.S.A.*
[b] *Dept. of Materials Science and Engineering, University of Wisconsin, Madison, WI 53706, U.S.A.*
[c] *Institute of Metallurgy, Clausthal University of Technology, D-38678 Clausthal-Zellerfeld, Germany*
[d] *Institute for Materials Research, University of Salford, Salford M5 4WT, U.K.*

Abstract. The newly enhanced PANDAT, integrating PanEngine, PanOptimizer and PanPrecipitation, bridges thermodynamic calculation, property optimization, and kinetic simulation of multi-component systems based on CALPHAD (CALculation of PHAse Diagram) approach. This software package, in combination with thermodynamic/kinetic/thermo-physical databases, provides an integrated workspace for phase diagram calculation and materials property simulation of multi-component systems. The simulation results, which include thermodynamic, kinetic, thermo-physical properties, and microstructure related information, are critically needed in materials design, in the selection of parameters for fabrication steps such as heat treatment, prediction of performance, and failure analysis. In addition to the functionalities provided by PANDAT as a stand-alone program, its calculation/optimization engines (PanEngine, PanOptimizer and PanPrecipitation) are built as shared libraries and enable their integration with broader applications in the field of Materials Science and Engineering.

Keywords: PANDAT, PanEngine, PanOptimizer, PanPrecipitation, CALPHAD, Phase Diagram Calculation, Materials Design, Thermodynamic Calculation Engine, Integrated Computational Materials Engineering (ICME), Materials Informatics.

1 INTRODUCTION

In 1996, Professor Y. Austin Chang founded CompuTherm LLC focusing on the development of a new generation of phase diagram calculation software - PANDAT. To date, PANDAT has been recognized as an intelligent (automatic calculation), reliable, robust and user-friendly software package and has been widely used in academia and industry in the field of Materials Science and Engineering.

In previously published articles [1, 2], Chen et al. have discussed some features of the earlier versions of PANDAT including the automatic calculation of stable phase equilibria without user-supplied initial values for a specific point (zero dimension), a line (one dimension) or a section (two dimensions). The features of the liquidus projection and solidification simulation for multi-component systems were also introduced.

In recent years, these features have been substantially enhanced. Moreover, the functionality has been significantly broadened and now PANDAT software has become an integrated computational environment for phase diagram calculation and materials property simulation of multi-component systems with good reliability, usability, extendability and intelligence. Some unique features are highlighted:

1) Intelligent/Reliable thermodynamic calculation engine: PANDAT's automatic thermodynamic calculation engine, PanEngine, can find the stable phase equilibria without requiring user-input initial values due to the use of specially designed global optimization algorithms. This feature has been greatly enhanced recently: on the one hand, the calculation speed has been improved five times on average while the

memory usage has been considerably reduced. On the other hand, specially designed constrained global optimization algorithms have been developed, which leads to the rapid solution of stable phase equilibrium not only for phases described with the traditional Solution, Line Compound or Compound Energy Formalism (CEF) models but also for those phases described by other complex models: the ionic liquid, the associate solution, CEF with ionic species models, as well as the more advanced Cluster/Site Approximation (CSA).

2) PanOptimizer for property optimization: a new module named PanOptimizer has been developed for the optimization of thermodynamic, kinetic and thermo-physical model parameters from known experimental or calculated data. This module is integrated with the PanEngine/PanPrecipitation modules and uses reliable/robust algorithms in finding an optimal set of parameters in terms of available experimental or calculated data. PanOptimizer reads the widely accepted POP format [3] for the experimental data, a feature which leads to its compatibility with other software package used for data assessments.

3) PanPrecipitation for precipitation simulation: The PanPrecipitation is a kinetic module designed for simulating precipitation kinetics during heat treatment processes. It is integrated into PANDAT as a built-in module that extends the capability of PANDAT for kinetic calculations, while taking full advantage of both the automatic thermodynamic calculation engine – PanEngine and the user-friendly PANDAT Graphical User Interface.

4) Calculation of material property: Many thermodynamic, kinetic and thermo-physical related properties can be computed by PANDAT. They are obtained by customizing the table columns in well-formatted table templates. These functions enable a range of exciting applications.

5) User-Friendly Graphical User Interface (GUI) and flexible input/output functions: PANDAT combines powerful calculation engines including PanEngine, PanOptimizer and PanPrecipitation with a user-friendly Microsoft Windows-based graphical interface. Complex calculations are completed with only a few mouse clicks. It is easy for a novice to use and effective for an expert. Besides carrying out calculations from the GUI, PANDAT also allows the user to run a series of calculations defined in a text/script file over an extended period through the "*Batch Calculation*" function. Furthermore, a variety of table and graph functions are provided for the user to create customizable and publication-quality graphs.

6) Integrated workspace: PANDAT provides a seamlessly integrated workspace for phase diagram calculation and materials property simulation. With one integrated workspace, the user can do all different types of calculations and organize the simulation results in a more convenient, consistent and reliable manner.

7) Good extendability: PANDAT is capable of incorporating a user's own thermodynamic/kinetic models to create custom applications. In addition to the functionalities provided in PANDAT as a stand-alone program, its calculation engines are built as shared libraries and enable their integration with other models for

broader applications in the framework of Integrated Computational Materials Engineering (ICME) or Materials Informatics [4-6].

In this paper, we will first introduce the overall architecture of PANDAT software and then focus on the newly enhanced/added features with regard to both its performance and functionality. Finally, feature functions of PanEngine and their integration with microstructure evolution types of models will also be discussed.

2 PANDAT

2.1 Architecture

PANDAT is modularly designed and currently composed of five major modules: PanSolver, PanEngine, PanOptimizer, PanPrecipitation and PanGUI (the Graphical User Interface). The module dependencies are shown in Figure 1. All the modules except the PanGUI are compiled and linked as shared libraries. PanSolver is a collection of C/C++ subroutines and functions for solving the local/global optimization and nonlinear algebraic/differential equations associated with phase equilibrium calculations and kinetic simulations. PanEngine accomplishes most of the calculations related to thermodynamics and phase equilibria. PanPrecipitation is a kinetic module designed for the simulation of precipitation kinetics during heat treatment processes. It is worth noting that users are able to integrate their own thermodynamic and kinetic models with PanEngine and PanPrecipitation, respectively. PanOptimizer is for evaluating thermodynamic, kinetic and thermo-physical model parameters based on either experimental measurements or theoretically calculated results. Finally, the integrated PanGUI accepts user's commands

with calculation conditions and displays the calculated results in the form of text, table or graph; customized output files may also be generated in the optional batch calculations.

As can be seen in Figure 2, PANDAT logically consists of three separate layers: the user interface layer, the calculation layer and the data layer. The top level of PANDAT is the user interface layer, whose purpose, as mentioned above, is to translate and pass the commands or calculation conditions to the calculation layer and then display the results returned from the calculation layer as texts, tables or graphs. The calculation layer processes the commands and conditions from the user interface layer, reads the model parameters stored in the data layer from thermodynamic, kinetic or thermo-physical databases and then performs the calculations. After calculation is done, it returns the calculation results to the user interface. This type of architecture leads to good extendability and maintainability of the PANDAT software. Its allowance for parallel development of each individual layer and having different experts focus on each of the three layers significantly increases the overall quality of PANDAT. More importantly, the modularly designed calculation layer (PanEngine, PanOptimizer, PanPrecipitation and PanSolver) can be re-used by other applications. This reduces any subsequent development efforts, minimizes the maintenance workload and decreases migration costs when switching client applications, e.g., from a conventional desktop application to a future web application.

2.2 The PANDAT Graphical User Interface (PanGUI)

The GUI of the PANDAT workspace consists of five components: Menus, Toolbars, Status Bar, Explorer Window and Main Display Window as shown in Figure 3.

The Menus provide commands for performing all types of calculations and other general operations such as opening and saving a workspace file (*.PND). The Toolbar buttons allow for accessing the frequently used menu commands. The Status Bar is located at the bottom of the workspace and provides a detailed description when the cursor is on the menu, toolbar button or graph. The Explorer Window lists the workspace contents, including any materials system information and simulation results in the current workspace. The contents are displayed in a tree structure. By clicking each tree node, the text, graph or table will be displayed in the Main Display Window. This provides both a clear track record of all calculations performed in that session and an easy access to each result.

2.3 PanEngine for Thermodynamic Calculations

In PANDAT, thermodynamic calculations are all performed in PanEngine. In the CALPHAD approach the Gibbs energies of phases in an alloy system are described by different thermodynamic models such as the random substitutional solution model, the stoichiometric compound model and the compound-energy-model (CEF) [7]. In addition to these commonly used models, PanEngine can also deal with both ideal and non-ideal gases, the ionic liquid model, the associate solution model, the CEF with ionic species and the more advanced Cluster/Site Approximation (CSA) [8-11].

2.3.1 Algorithms for Global Minimization

In order to solve the phase equilibrium problem for a multi-component system, minimization of the Gibbs energy functions described with different thermodynamic models is a pre-requisite. However, due to the complexity of the models and the possible

presence of multiple solutions, the algorithms available in most commercial software packages provide no guarantee of obtaining the correct solution for the general phase equilibrium problem. By using such software, the user cannot obtain the global stable phase equilibrium unless proper initial values are specified. This situation is exaggerated if a more complicated model such as the CEF with ionic species or the CSA is used in a multi-component system.

Faced with this problem, a special global optimization algorithm was implemented in PanEngine by Chen et al. [1], which has been proved to be very successful in multi-component phase diagram calculation. Due to the implementation of this algorithm, PanEnigine has a unique ability in calculating unknown phase diagrams without requiring any starting guesses or information about the likely presence of the most stable phase in the system of interest.

Recently, considerable effort has been made in enhancing the global optimization algorithms in PanEngine. As a result, PanEngine has become even more reliable and efficient in finding the global stable phase equilibria. This point can be illustrated by the following two examples.

In the first example, a series of randomized test functions [12] are used to quantitatively evaluate the reliability and efficiency of the global optimization algorithms available in PanEngine. These tests are formulated as,

$$f(x) = s\sum_{i=1}^{n}\left(x_i - x_i^*\right)^2 + \sum_{k=1}^{k_{\max}} a_k \sin^2\left[f_k P_k\left(x_i - x_i^*\right)\right] \qquad (1)$$

where n is the number of the variables and x^* is the randomly generated unique global solution chosen from a uniform distribution on interval [-5, 5]. $s = 0.025 * n$ is the scaling factor. While $a_k = 1, f_k = 0.5$ $(k = 1,...,k_{\max})$ are the amplitude scalars and frequency multipliers. $k_{\max} = 2$ is chosen throughout the evaluation. The two equations $P_1(x - x^*) = \sum_{i=1}^{n}(x - x^*) + \sum_{i=1}^{n}(x - x^*)^2$ and $P_2(x - x^*) = \sum_{i=1}^{n}(x - x^*)$ are polynomial noise terms with the required properties. For illustration, a randomly generated instance of such test functions in the two-dimensional cases is shown in Figure 4, where the test function is inverted so as to be visualized more clearly, i.e., the objective $-f(x)$ is maximized. In addition to the unique global optimum value of 0 at $x_1^* = 0.9913937803$ and $x_2^* = -1.724448378$, the test functions present a large number of local optima, which lead to non-trivial test problems.

The test functions are solved by utilizing the global optimization algorithms in PanEngine for cases of n = 1, …, 10 and the results are summarized in Table 1. It can be seen that the optimal values are all found up to at least 1e-10 precision in terms of the theoretical optimum value of 0 in less than 20 milliseconds with the number of function evaluations ranging from a few hundreds to a few thousands. It is to be noted that all the tests, including the benchmarks being presented in the next section, are performed on an Intel Core2 2.0 GHz personal computer with a Windows XP Professional Version operating system.

The second example concerns the calculation of the binary Fe-O phase diagram and an isothermal section of Fe-Cr-O system at 1573K and its corresponding stability

diagram. The calculated phase diagrams are shown in Figures 5, 6 and 7, respectively. It should be pointed out that the spinel phase in these systems is described with a four sublattice CEF model which has many end-members with ionic species on the sublattices. The model for the multi-component system is, therefore, especially complex and the minimization of the Gibbs energy function is rather challenging. This is particularly true in finding the most stable phase equilibrium using the global optimization algorithm since many extra constraints are introduced in order to maintain electro-neutrality. Notwithstanding the complexity of the thermodynamic models used, PanEngine is able to find the stable phase equilibria and calculate the correct phase diagrams in a purely automatic manner. The whole calculation does not require the user to provide any initial values.

2.3.2 Performance

In addition to the enhanced optimization algorithms, the numerical algorithms for one/two dimensional mapping, liquidus projection and solidification simulation, as well as the data structures in PanEngine have been greatly improved in PANDAT 7. This has resulted in five times improvement of the overall calculation speed on average, while the memory usage has been significantly reduced.

A benchmark has been carried out for the calculation of 148 binary phase diagrams. The total calculation time for PANDAT 7 and PANDAT 5 is compared in Table 2. It indicates that PANDAT 7 is about four times faster than PANDAT 5 in calculating a total of 148 binary phase diagrams, while only half memory space is needed. Noting the fact that most of the binary systems are calculated in a few seconds and the

post-possessing time (retrieving tables and plotting graphs) requires a significant fraction of the total time; the improvements in performance for complex multi-component systems are even better. This can be illustrated by the following benchmarks for calculations on Ni-based and Nb-based alloys, in which the PanNickel and PanNiobium databases, developed by CompuTherm, were used.

The first benchmark is for a point calculation of the Nickel 625 alloy containing 9 components at 663°C. In order to do the point calculation, as mentioned in literature [1], the user must define the temperature, pressure and overall composition of the alloy. It is worth mentioning that PANDAT 7 provides functions for defining a materials system with user-defined alloys. This allows the user to quickly set up the calculation conditions without having to manually type in the alloy composition for each component. The calculated results are presented in Figure 8 (a) as a list table and Figure 8 (b) as a grid table, respectively. Another benchmark has been carried out for a line calculation of the Nickel 718 alloy with 9 components from 1500°C to 600°C and the calculation result is plotted in Figure 9. In addition, several section calculations have been carried out for the binary Ni-Al system and the ternary Ni-Al-Pt and Ni-Al-Ru systems. The calculated phase diagrams are shown in Figures 10, 11 and 12, respectively. The results of a liquidus projection for the Ni-Al-Ir system and solidification simulations under the Lever Rule and Scheil conditions for a niobium alloy (Nb-22Ti-2Hf-4Cr-3Al-16Si in at%) are presented as well in Figures 13 and 14. It should be pointed out that all these calculations have been performed on the same hardware platform, operating system and software environment for both PANDAT 7 and PANDAT 5. The generated benchmark results in

Table 2 clearly show that the performance of PANDAT 7 has been improved around five times on average over PANDAT 5.

2.4 PanOptimizer for Data Assessments

PanOptimizer has been developed for evaluating not only the thermodynamic but also the kinetic and thermo-physical model parameters from experimental or theoretically calculated data [8]. It is dynamically linked with PanEngine and seamlessly integrated into PANDAT as a specific module, which allows the user to make real-time calculations and comparison with the experimental data based on the instantly optimized parameters. A set of Windows-based graphical user interfaces are deliberately designed for convenient input/output of the experimental data and the parameters being optimized. The functions for automatic tracking of the optimization progress are also provided.

2.4.1 Normal Optimization

Derived from the maximum likelihood principle, when the discrepancies between model-calculated and experimental values are assumed to be independent, identically distributed with a normal distribution function, a set of model parameters with the best fit to the given experimental data can be obtained by minimizing the sum of squares (the least squares method). In the real modeling process the experimental data may come from different sub-populations for which an independent estimate of the error variance is available. In this case, a better estimate than the ordinary least squares can be obtained by using the weighted least squares, also called generalized least squares. In this case, the sum of the squares can be written as

$$\frac{1}{2}\sum_{j=1}^{m} w_j \left[e_j - \phi(p; T_j, x_j) \right]^2 \qquad (2)$$

where the e_j are the experimentally measured values, m is the total number of values being measured. The "model function" is written as $\phi(p; T, x)$. T and x define a point in the state space with T being the temperature and x the alloy composition, while p is a vector of parameters in the thermodynamic models. The idea is to assign each observation a weight factor w_j which reflects the uncertainty of the measurement. This method has proved to be quite efficient and reliable in the real modeling process.

In order to do the optimization, a user first defines the model parameters to be optimized. PanOptimizer asks the user to define the optimization parameters in the TDB file. Additionally, the user must provide the experimental/calculated data. In the CALPHAD community, a commonly adopted format for presenting experimental data is the POP file. PanOptimizer reads most of the keywords in the POP format but extends its use for additional optimization functions.

In PanOptimizer, the optimization is operated through a control panel, which provides a series of functions for controlling and tracking the optimization process. A screen image of the control panel is captured and shown in Figure 15. Not only does it contain a "Histogram" window for displaying and tracing the history of the discrepancy between model-calculated values and experimental data, but it also provides functions for directly reviewing the optimized model parameters or the model calculated values compared with the experimental data. During the optimization procedure, the user is able to adjust the parameter information including the lower and upper bounds and initial

values as needed. Similarly, the experimental information such as uncertainty and weight factor can be adjusted as well. Since PanOptimizer is seamlessly integrated with PANDAT as a specific module, i.e., in the same workspace, the user can utilize all other functions available in PANDAT to make real-time calculations and comparisons with the experimental data based on the instantly optimized parameters. This leads to the entire optimization process being accomplished in a more convenient and efficient manner.

As an illustration, PanOptimizer is used to optimize the binary Al-Zn system [8]. The three files mentioned in this section are “AlZn_Sample.tdb”, “ALZN_Sample.pop” and “ALZN_Sample_Rough.pop”, which can be found in the standard installation folder of PANDAT 7.

The 11 model parameters to be optimized are first defined in “AlZn_Sample.tdb” and their initial values are all set to be zero. The available experimental data of the system include the enthalpy of the liquid phase at 953 K, two invariant reactions at 655 K: LIQUID -> FCC_A1 + HCP_A3 at 550 K: FCC_A1#2 -> FCC_A1#1 + HCP_A3, and tie-lines for FCC_A1#1 + FCC_A1#2, LIQUID + FCC_A1, LIQUID + HCP_A3 and HCP_A3 + FCC_A1 at different temperatures. These data are then defined in the POP file named as “ALZN_Sample.pop”.

Before the optimization, the Al-Zn phase diagram and the enthalpy of the liquid phase at 953 K are calculated and plotted together with the experimental data in Figures 16 (a) and (b), respectively. Large discrepancies between the calculated values and the experimental data are observed. The optimization is thus performed with PanOptimizer. After several rounds of optimization, the sum of squares decreases from 904896 to 2.8.

The subsequent calculations are carried out based on the instantly optimized parameters and the comparisons in Figure 17 indicate that excellent agreement has been achieved.

2.4.2 Rough Search

"Rough Search" is used to obtain a rough topology of a phase diagram based on the given experimental data. It can be useful for quickly estimating the initial values of the model parameters at the beginning stage of the optimization procedure. The algorithm used by PanOptimizer to do "Rough Search" is based on the *necessary* (*but not sufficient*) condition of equilibrium among the specified phases in a closed system at constant P and T:

$$\mu_C(i) = \mu_C(j) \text{ for any component } C \text{ in any two phases } i, j \qquad (3)$$

For each pair of two phases (i and j) in equilibrium, if the tie-line information is available, $\mu_C(i)$ and $\mu_C(j)$ can be calculated at the equilibrium compositions using the selected thermodynamic models and the initial model parameters. The "Rough Search" will find a set of model parameters that give the best fit to the experimental phase boundary data by minimizing the chemical potential differences between the two speficified phases in equilibrium, and the least squares problem is then written as:

$$\frac{1}{2}\sum_{k=1}^{m} w_k \sum_{C}\left[\frac{\mu_C(i)-\mu_C(j)}{RT_k}\right]^2 \qquad (4)$$

where w_k is a weight factor that reflects the uncertainty of the measurement for equilibrium k, i and j represent any two phases in k^{th} equilibrium. The idea of "Rough Search" is now illustrated by using the Al-Zn system again. Figures 18 (a) and (b) are

phase diagrams calculated before and after the rough search, respectively. Similarly, Figures 18(c) and 18(d) plot the Gibbs energy functions for phases FCC_A1 and HCP_A3 at 500 K. The compositions of the experimental tie-lines between these two phases are also highlighted in the phase diagrams for comparison. As can be seen, large differences for the chemical potentials of Al and Zn between the two phases are observed in Figure 18(c) before the rough search. The differences diminish to be nearly zero after the rough search as shown in Figure 18(d) and the calculated phase equilibrium agrees well with the given experimental data. The advantage of "Rough Search" compared to "Normal Optimization" is that it does not directly involve tie-line data; it therefore works even if a tie-line does not exist with the current ("rough") set of thermodynamic parameters.

In addition to the phase boundary data, the thermodynamic properties for the single-phase equilibrium can also be included for the rough search. Therefore, the final least squares problem for the rough search is written as:

$$\frac{1}{2}\sum_{k=1}^{m} w_k \sum_{C}\left[\frac{\mu_C(i)-\mu_C(j)}{RT_k}\right]^2 + \frac{1}{2}\sum_{j=1}^{n} w_j \left[e_j - \phi(p;T_j,x_j)\right]^2 \qquad (5)$$

The meaning of the second term in equation (5) is the same as that in equation (2) except that it refers only to the thermodynamic properties of a single-phase.

There are two types of built-in optimization algorithms for "Rough Search", which are "Global Search" and "Local Search". "Global Search" is for searching a set of good initial values of the model parameters within the whole search domain, while "Local Search" leads to a quick convergence to an optimal solution based on the given

initial values of the model parameters. Either way, the resulting parameters of the "Rough Search" provide useful initial parameter values for the "Normal Optimization" described in section 2.4.1.

2.4.3 Applications

The application of PanOptimizer is not limited to simple binary systems. To date, it has been used for many multi-component systems described with the complex CEF and CSA, e.g., Ni-Al-Cr [13], Ni-Al-Ir [14], Ni-Al-Ru [15], Ni-Al-Pt [16], Hf-Ti-Si [17], Cr-Hf-Si, Cr-Nb-Si, Mo-Si-B-Ti to name a few.

As pointed out at the outset, PanOptimizer is designed not only for thermodynamic data assessments, but also for the development of databases needed by other applications such as for kinetic simulation or thermo-physical modeling. Such an example is given later in Figure 27 for optimizing mobility parameters. In this example, the mobility parameters of the γ phase in Ni-Al are optimized in terms of the inter-diffusion coefficients measured at different temperatures and compositions. Good agreement between the calculated values and the experimental data is obtained after the optimization.

2.5 PanPrecipitation for Kinetic Simulations

PanPrecipitation is designed for simulating precipitation kinetics during heat treatment processes. It is built as a shared library and integrated into PANDAT as a specific module that extends the capability of PANDAT for kinetic simulations, while taking full advantage of the automatic thermodynamic calculation engine (PanEngine)

and the user-friendly PANDAT Graphical User Interface (PanGUI). And for this reason, precipitation simulations for highly complex alloys under arbitrary heat treatment conditions can be accomplished with only a few operations.

2.5.1 Data Structure

PanPrecipitation is a purely object-oriented module written in C++ with generic data structures like PanEngine, balancing performance, maintainability and scalability. The basic data structure for storing precipitation information in the system of interest is schematically shown in Figure 19. In general, a system contains a matrix phase and a number of precipitate phases. The precipitation behavior of different precipitate phases can be described by different kinetic models. In addition to the two built-in models: the Kampmann/Wagner Numerical (KWN) [18] model and the Fast-Acting model [19], the generic data structure as shown in Figure 19 also, and importantly, enables its integration with user-defined kinetic models.

Based on the above data structure, input parameters for the matrix and its precipitate phases are organized in “Extensible Markup Language” (XML) format, which is a standard markup language and well-known for its extendability. In accordance with the XML syntax, a set of well-formed tags are specially designed to define the kinetic model for each precipitate phase and its corresponding model parameters like interfacial energy, molar volume, nucleation type, morphology type, and so on. As mentioned earlier, there are two built-in kinetic models known as the KWN and Fast-Acting already implemented in PanPrecipitation. Both models can be used to simulate the co-precipitation of phases with various morphologies, with concurrent processes of

nucleation, growth and coarsening. With the selection of the KWN model, the particle size distributions (PSD) of various precipitate phases can be obtained in addition to the temporal evolution of the average size and volume fraction as obtained from the Fast-Acting model.

2.5.2 Kinetic Models

In PanPrecipitation, KWN model is based on the Kampmann and Wagner's work as implemented in a numerical framework [18], and extended to handle both homogeneous and heterogeneous nucleations, dealing with various morphologies for the simulation of co-precipitation kinetics of multi-component alloys under arbitrary heat treatment conditions. The following is a brief introduction to the KWN model along with its sub-models for nucleation, growth and coarsening. More detailed descriptions can be found in Refs. [18, 20, 21].

Specifically, in the KWN model the continuous PSD is divided into a large number of size classes. The program takes a simulation step at every sample time hit. To maintain both accuracy and efficiency between two adjacent simulation steps, a fifth-order Runge-Kutta scheme is used to generate an adaptive step size based on the continuity equation.

At each simulation step, the number of new particles is first calculated using classical nucleation theory and then these new particles are allocated to an appropriate size class. The transient nucleation rate is given by,

$$J = N_v Z \beta^* \exp(-\frac{\Delta G^*}{kT}) \exp(\frac{-\tau}{t}) \qquad (6)$$

where $\Delta G^* = \frac{4\pi}{3}(R^*)^2\sigma$. R^* is the radius of the critical nucleus and $R^* = \frac{-2\sigma}{\Delta G_V}$. ΔG_V is the chemical driving force for nucleation and σ is the interfacial energy of the matrix/particle interface. The pre-exponential terms in equation (6) are: N_v, the nucleation site density, Z, the Zeldovich factor and β^*, the atomic attachment rate. t is the time, τ the incubation time for nucleation, k the Boltzmann constant and T the temperature. The multi-component version of the parameters has been proposed by Kozeschnik et al. [22] and implemented in PanPrecipitation. The nucleation site density and nucleation driving force are modified to deal with heterogeneous nucleation.

Next, the growth of existing particles for each size class is computed by assuming diffusion-controlled growth, where the Gibbs-Thomson size effect is also taken into account. The growth model for multi-component alloys proposed by Morral and Purdy [23] is adopted in PanPrecipitation and modified to handle the growth/dissolution of various precipitate phases with different morphologies. The motion rate of the curved interface, e.g., the interface of a spherical or lens-like precipitate, and the edge of a plate-like precipitate, is given by,

$$v = \frac{dR}{dt} = \frac{K}{R}\left(\frac{1}{R^*} - \frac{1}{R}\right) \tag{7}$$

with

$$K = \frac{2\sigma V_m}{\left(\Delta C^{\alpha\beta}\right]\left[M\right]^{-1}\left[\Delta C^{\alpha\beta}\right)} \tag{8}$$

where R is the radius of the interface, R^* is the radius of the critical nucleus and σ being the interfacial energy between matrix (α) and precipitate phase (β), V_m being the molar volume of the precipitate phase, $\left(\Delta C^{\alpha\beta}\right]$ and $\left[\Delta C^{\alpha\beta}\right)$ being the row and column vector of the solute concentration difference between α and β, and $[M]$ being the chemical mobility matrix. The motion rate of the planar interface, e.g., thickening of the plate, is described by

$$v = \frac{dh}{dt} = \frac{K'}{h} \tag{9}$$

with $K' = \dfrac{\Delta G_m^*}{\left(\Delta C^{\alpha\beta}\right][M]^{-1}\left[\Delta C^{\alpha\beta}\right)}$, where h is the half thickness of the plate and ΔG_m^* is the transformation driving force.

Finally, the PSD and the volume fraction of the particles are updated and the matrix composition is recalculated based on mass conservation equation (10) in the end of each simulation step. The updated values are then used in the next time step.

$$C_i^* = \left(1 - \sum_P^{n_P} \phi_P\right) C_i^\alpha + \sum_P^{n_P} \phi_P C_i^P \tag{10}$$

where C_i^* is the initial mole fraction of component i, ϕ_P is the mole fraction of precipitate phase P, n_P is the number of precipitate phases, C_i^α is the mole fraction of component i in the matrix phase α, and C_i^P is the mole fraction of component i in precipitate phase P.

It should be noted that coarsening in the KWN model arises naturally and becomes dominant when the supersaturation is sufficiently low. In the Fast-Acting model, however, the coarsening is considered explicitly. Accordingly, a model based on the LSW theory [24, 25] is employed, which characterizes the curvature-driven particle growth. The multi-component version can be written as,

$$\bar{R}^3 - \bar{R}_0^3 = \frac{4}{9} Kt \qquad (11)$$

Where $\bar{R}$ is the average particle radius at time t, $\bar{R}_0$ is the average particle radius at the onset of coarsening and K is the kinetic parameter defined in equation (8). Its accuracy and efficiency are ensured by controlling the adaptive step size with a fifth-order Runge-Kutta scheme. At each simulation step, the same nucleation and growth models, as given in equations (6), (7) and (9), are used for the estimation of the average size changes. It is worth pointing out that the thermodynamic equilibrium information, the driving force and the diffusivity data needed for both KWN and Fast Acting simulations are obtained by directly coupling with the automatic thermodynamic calculation engine – PanEngine. Therefore, no initial values are required for the thermodynamic calculation at every simulation step. This makes PanPrecipitation very reliable and user-friendly in the simulation of precipitation kinetics, especially for multi-component alloys.

2.5.3 Example

As a validation, PanPrecipitation was used to simulate the kinetics of precipitation in a Ni-14 at% Al alloy isothermally annealed at 550°C. This example has been studied previously by Kampmann and Wagner [18]. Two simulations were carried out based on

the built-in KWN and Fast-Acting models, respectively. The PanNickel 7 database was used for both simulations. This database provides the relevant thermodynamic model parameters and mobility data. The input parameters for kinetic models – the interfacial energy, the nucleation site density were optimized in terms of the measured number density and average particle size [26].

Figure 20 plots the evolution of the average γ' particle size with aging time obtained from the KWN and Fast-Acting models. Figure 21 and Figure 22 show, respectively, the KWN-predicted evolution of particle number density and supersaturation, superimposed with the experimental data. As can be seen, the predictions and the measurements are in reasonable agreement.

The KWN-predicted γ' size distributions for the alloy after aging at 550°C for 21, 217 and 3720 minutes are shown in Figure 23. These distributions are plotted in terms of the particle frequency, which is computed by normalizing the total number of particles to be one. At the early stages of the precipitation, the nucleation process is dominant and the number density of γ' particles increases rapidly. Therefore, the PSD is characterized by a sharp peak around the critical nucleus size as shown in Figure 23 for t = 21 minutes. At the later stages, the transformation falls into the coarsening regime and the PSD is then flattened as indicated in the case of t = 3720 minutes. It is interesting to point out that the PSD, at an intermediate stage of t = 217 minutes, displays a double peak. This phenomenon, however, is consistent with the previous findings from both experimental observation [27] and model prediction [20].

2.6 Calculation of Materials Property

As pointed out in section 1, PANDAT combines the automatic thermodynamic calculation engine (PanEngine), the data assessment/optimization module (PanOptimizer) and the kinetic simulation module (PanPrecipitation) with the user-friendly graphical user interface (PanGUI). All types of calculations such as point, line, section, liquidus projection, solidification simulation and kinetic simulation, can be accomplished with a few operations. Upon the completion of each simulation, one or more tables with related properties and one graph are created by default. However, it should be emphasized here that, in addition to the default tables, variety of properties, such as phase amount, activity, Gibbs energy, enthalpy, entropy, heat capacity, molar volume, density, surface tension, viscosity, and diffusivity, can be retrieved through "Edit Table". Accordingly, a variety of property diagrams can be generated based on the customized tables, which offers users a good flexibility for different applications. A few examples are given below.

The first example is a phase amount *vs.* temperature diagram, which is shown in Figure 9. The diagram shows the phase fraction of each phase in thermodynamic equilibrium as a function of temperature. Such information is useful in understanding the microstructure of a material obtained under different heat treatment conditions, and is critically needed in the selection of parameters for the heat treatment of an alloy.

Figure 24 illustrates an activity *vs.* composition diagram, which is obtained by first doing a line calculation from pure Al to pure Ni in the Ni-Al system at 1700 K and then customizing the default table to get the activities of each element using FCC_A1 as the reference state. In addition to the properties of stable phases, PANDAT is capable of

calculating the thermodynamic properties of each individual phase separately regardless of their stability. Needless to say, this function is very useful in assisting users to understand the properties of each phase and visualize their relative stability. As an illustration, a calculation was carried out for the Ni-Al system at 1700 K for the Liquid, B2 and FCC_A1 phases. The calculated Gibbs energies are plotted in Figure 25 as a function of mole fraction of Ni. The relative stability of these three phases are clearly seen in this plot, and is consistent with the stable phase diagram of Figure 10 and the activity plot in Figure 24.

In addition to the thermodynamic properties, thermo-physical properties, such as molar volume, density, surface tension and viscosity, can be easily calculated by PANDAT as well. As an example, a density vs. temperature diagram for alloy Al-7075-T6 (Al-0.2Cr-1.6Cu-0.5Fe-2.5Mg-0.3Mn-0.4Si-0.2Ti-5.6Zn in wt%) is calculated as shown in Figure 26. In diffusion control processes, mobility data are critically needed. One new feature of PANDAT 7 is that it allows the calculation of tracer diffusivity and inter-diffusivity through “Edit Table”. This requires, of course, that the mobility model parameters being developed first and stored in the database. Figure 27 shows the calculated inter-diffusion coefficients of binary Ni-Al alloys as a function of Al content at various temperatures. The experimental data were also plotted on the figure for comparison.

3 INTEGRATION WITH PANENGINE

While the focus has been placed previously on demonstrating the functionalities of PANDAT as a stand-alone program, this part is devoted to the introduction of its

integration with broader applications in the framework of Integrated Computational Materials Engineering (ICME) or Materials Informatics [4-6]. Since PANDAT's calculation/optimization engines including PanEngine, PanOptimzer and PanPrecipitation are packaged as shared libraries, they give the user complete control over their functions in a more manageable and intuitive programming style with less overhead and complexities. This greatly simplifies their integrations with other applications. As an illustration, the integration with PanEngine will be discussed in the following. The integration with the other libraries can be fulfilled in a similar way, thus no further discussion is given here.

3.1 Features of PanEngine

PanEngine is a Dynamic Link Library (DLL), which is a collection of functions for calculating thermodynamic, thermo-physical properties and phase equilibrium for a multi-component, multi-phase system. As emphasized earlier, PanEngine finds the correct, stable phase equilibria without requiring the user to input initial values. This unique feature becomes especially important when integrating with other applications, since it is impossible for the user to enter initial values and verify results when a custom software program needs stable phase equilibrium information for thousands of points during the simulation. On the other hand, for multi-component systems, it is extremely difficult, if not impossible, to guess the initial values for stable phase equilibria.

PanEngine provides many commonly used functions, which can be directly accessed by user's applications. The major functions are listed below:

1) Load Database: PanEngine loads databases in TDB or PDB format. A database contains the parameters for thermodynamic, thermo-physical and kinetic properties of phases in a multi-component system.

2) Select Components: Information for a subsystem can be extracted from a database by setting the subsystem components.

3) Suspend/Restore Phases: This function suspends or restores phases in a system.

4) Switch Composition Units: This function switches compositions between mole fraction/percentage and weight fraction/percentage.

5) Calculate Stable Equilibrium: For a given temperature and overall composition or for a fixed partial pressure of gas species, PanEngine calculates the most stable phase equilibrium. In order to calculate a metastable equilibrium, the “suspend” function can be used to suspend some more stable phases.

6) Calculate Local Equilibrium: If only a local phase equilibrium is required, PanEngine has an option to calculate the local equilibrium without examining its stability using a previously calculated equilibrium as the initial value.

7) Find Liquidus Surface: A liquidus surface can be found for a given overall composition of a system.

8) Calculate Liquidus Slope: A liquidus slope along the direction of a specified component can be calculated for a given overall composition.

9) Calculate Partition Coefficient: This function calculates the partition coefficient of a component between two phases in equilibrium.

10) Calculate Thermodynamic Factor: This function calculates the thermodynamic factor, i.e., the gradient of chemical potential of a component. It is an important property for diffusion simulation.

11) Simulate Solidification Using Scheil, Lever Rule or User-Defined Models: There are two built-in models available in the solidification simulation functions: Scheil and Lever Rule. Thermodynamic and thermo-physical properties, such as the solid phase fractions, heat capacity and latent heat, are stored in an object of a class at each simulation step. In addition, the specially designed solidification functions in PanEngine provide users with a flexible option which enables them to incorporate their own solidification models.

All these functions can be accessed and integrated with user's codes to create custom software applications, such as microscopic/macroscopic solidification simulations, heat treatment simulations and other applications where phase equilibrium information and thermodynamic properties are needed.

3.2 Integration with PanEngine

In order to facilitate user's applications of accessing the functions available in PanEngine, an object-oriented data structure has been deliberately designed and is schematically shown in Figure 28. In PanEngine, as can be seen in the figure, PanPoint which is directly interfaced with the user's application refers to a system with specified

composition, temperature and pressure. The user can define a “system” (temperature, pressure and overall composition) and retrieve related thermodynamic properties and phase equilibrium information of this “system” through the PanPoint object. The stable (or metastable) phase equilibrium information related to each phase, such as phase fractions, phase compositions, and thermodynamic properties of each phase, are stored in PanPhasePoint, while general information of the system, such as components, overall composition and temperature are stored in PanStateSpace.

With this data structure, it is easy for the user to access the needed information and build their own applications. In the following example, a modified two-dimensional cellular automaton (MCA) model is coupled with PanEngine [28] to simulate the microstructure and microsegregation of multi-component Al-Cu-Mg alloys during solidification.

In this application, the two key thermodynamic parameters needed for the simulation are the solute partition coefficient and the liquidus slope. For a simple binary alloy system, they are usually conveniently taken as constants. However, for multicomponent systems, such a treatment is no longer valid since the actual values of these quantities may vary significantly with temperature and compositions. This necessitates the integration of the simulation with a thermodynamic calculation engine.

The MCA model, in this regard, is coupled with PanEngine for the prediction of microstructures and microsegregation in the solidification of aluminum alloys. For illustration, several simulation results are presented here, which have been previously published in literature [28]. Figure 29 demonstrates the simulated dendrite morphology

and composition fields of two solutes, copper and magnesium, for an Al-15%Cu-1%Mg alloy in wt%. In this case, the cooling rate is 10K/s, and the ending temperature is the binary eutectic temperature of 810K. Figure 30 shows a comparison between the experimental microstructure and the simulated dendritic morphology of an Al-3.9%Cu-0.9%Mg alloy in wt%. The simulation was carried out in a domain consisting of 300×300 cells with a cell size of 3μm. The temperature of the domain was assumed to be uniform and cooled down from the liquidus temperature of 919 K to the binary eutectic temperature of 792 K with a constant cooling rate of 0.78 K/s.

4 CONCLUSIONS

The PANDAT software package, with PanEngine for thermodynamic calculation, PanOptimizer for property optimization and PanPrecipitation for precipitation simulation, is presented in this paper. The greatly enhanced performance and significantly broadened functionalities of PANDAT provide an integrated computational environment for materials property simulation of multi-component systems with good reliability, usability, extendability and intelligence. Its unique features such as efficient global optimization, automatic thermodynamic calculation, reliable optimization of model parameters and kinetic simulation have been demonstrated by a number of examples.

In addition to the functionalities provided by PANDAT as a stand-alone program, its integration with broader applications in the field of Materials Science and Engineering has also been discussed. An example to integrate PanEngine with a two-dimensional modified cellular automaton model has been given for the simulation of microstructure and microsegregation of aluminum alloys during solidification.

5 ACKNOWLEDGMENTS

We wish to acknowledge the financial support of US Air Force through the SBIR projects. We would especially like to thank Dr. Jeff Simmons and his colleagues of the AFRL at Wright-Patterson for their continuing interest in this work.

6 REFERENCE

1. Chen, S.L., S. Daniel, F. Zhang, Y.A. Chang, X.Y. Yan, F.Y. Xie, R. Schmid-Fetzer, and W.A. Oates, *The PANDAT software package and its applications.* Calphad-Computer Coupling Of Phase Diagrams And Thermochemistry, 2002. **26**(2): p. 175-188.
2. Chen, S.L., F. Zhang, S. Daniel, F.Y. Xie, X.Y. Yan, Y.A. Chang, R. Schmid-Fetzer, and W.A. Oates, *Calculating phase diagrams using PANDAT and PanEngine.* Jom-Journal Of The Minerals Metals & Materials Society, 2003. **55**(12): p. 48-51.
3. Andersson, J.O., T. Helander, L. Höglund, P.F. Shi, and B. Sundman, *Thermo-Calc and DICTRA, Computational tools for materials science.* Calphad-Computer Coupling Of Phase Diagrams And Thermochemistry, 2002. **26**: p. 273-312.
4. Allison, J., D. Backman, and L. Christodoulou, *Integrated Computational Materials Engineering: A New Paradigm for the Global Materials Profession.* Jom-Journal Of Metals, 2006. **58**(11): p. 25-27.
5. Liu, Z.-K., L.-Q. Chen, and K. Rajan, *Linking Length Scales via Materials Informatics.* Jom-Journal Of Metals, 2006. **58**(11): p. 46-50.
6. Rajan, K., *Materials Infomatics.* Materialstoday, 2005. **8**(10): p. 38-45.
7. Hillert, M., *The compound energy formalism.* Journal of Alloys and Compounds, 2001. **320**(2): p. 161-176
8. Cao, W., *Application of the Cluster/Site Approximation to Calculation of Multicomponent Alloy Phase Diagrams and Coherent Interphase Energies*, in *Materials Science and Engineering Department*. 2006, University of Wisconsin - Madison: Madison, WI. p. 214.
9. Cao, W., Y.A. Chang, J. Zhu, S. Chen, and W.A. Oates, *Application of the cluster/site approximation to the calculation of multicomponent alloy phase diagrams.* Acta Materialia, 2005. **53**(2): p. 331-335.
10. Oates, W.A. and H. Wenzl, *The cluster/site approximation for multicomponent solutions - A practical alternative to the cluster variation method.* Scripta Materialia, 1996. **35**(5): p. 623-627.
11. Oates, W.A., F. Zhang, S.L. Chen, and Y.A. Chang, *Improved cluster-site approximation for the entropy of mixing in multicomponent solid solutions.* Physical Review B, 1999. **59**(17): p. 11221-11225.
12. Pardalos, P.M. and H.E. Romeijn, eds. *Handbook of Global Optimization*. Vol. 2. 2002, Kluwer Academic Publishers: Boston/Dordrecht/London.
13. Cao, W., J. Zhu, Y. Yang, F. Zhang, S. Chen, W.A. Oates, and Y.A. Chang, *Application of the cluster/site approximation to fcc phases in Ni-Al-Cr system.* Acta Materialia, 2005. **53**(15): p. 4189-4197.
14. Zhang, C., J. Zhu, A. Bengtson, D. Morgan, F. Zhang, W. Cao, and Y.A. Chang, *Modeling of Phase Stability of the fcc Phases in the Ni-Ir-Al System Using the Cluster/Site Approximation Method Coupling with First-principles Calculations.* Acta Materialia, 2008. **Accepted**.

15. Zhu, J., C. Zhang, W. Cao, Y. Yang, F. Zhang, S.-L. Chen, D. Morgan, and Y.A. Chang, *Experimental Investigation and Thermodynamic Modeling of the Ni-Al-Ru System.* Acta Materialia, under review, 2008.
16. Zhu, J. and Y.A. Chang, *Experimental Investigation and Thermodynamic Modeling of the Ni-Al-Pt System.* In preparation, 2008.
17. Yang, Y., B.P. Bewlay, and Y.A. Chang, *Thermodynamic modeling of the Hf–Ti–Si ternary system.* Intermetallics, 2007. **15**(2): p. 168-176.
18. Kampmann, R. and R. Wagner, *Kinetics of Precipitation in Metastable Binary Alloys - Theory and Application to Cu-1.9at%Ti and Ni-14at%Al.* Decomposition of alloys: the early stages, ed. P. Haasen, et al. 1984, Oxford: Pergamon Press. 91-103.
19. Langer, J.S. and A.J. Schwartz, *Kinetics of nucleation in near-critical fluids.* Physical Review A, 1980. **21**(3): p. 948-958.
20. Robson, J.D., *Modelling the evolution of particle size distribution during nucleation, growth and coarsening.* Materials Science And Technology, 2004. **20**: p. 441-448.
21. Robson, J.D., M.J. Jones, and P.B. Prangnell, *Extension of the N-model to predict competing homogeneous and heterogeneous precipitation in Al-Sc alloys* Acta Materialia, 2003. **51**(5): p. 1453-1468
22. Kozeschnik, E., I. Holzer, and B. Sonderegger, *On the Potential for Improving Equilibrium Thermodynamic Databases with Kinetic Simulations* Journal Of Phase Equilibria and Diffusion, 2007. **28**(1): p. 64-71.
23. Morral, J.E. and G.R. Purdy, *Particle Coarsening in Binary and Multicomponent Alloys.* Scripta Metallurgica Et Materialia, 1994. **30**(7): p. 905-908.
24. Lifshitz, I.M. and V.V. Slyozov, *The kinetics of precipitation from supersaturated solid solutions.* J. Phys. Chem. Solids, 1961. **19**: p. 35.
25. Wagner, C., *Theorie der Alterung von Niederschlägen durch Umlösen (Ostwald-Reifung).* Z. Elektrochem., 1961. **65**: p. 581.
26. Wendt, H. and P. Haasen, *Nucleation and growth of γ'-precipitates in Ni-14 at. % Al.* Acta Metallurgica et Materialia, 1983. **31**(10): p. 1649-1659.
27. Xiao, S.Q. and P. Haasen, *HREM investigation of homogeneous decomposition in a Ni-12 at. % Al alloy.* Acta Metallurgica et Materialia, 1991. **39**(4): p. 651-659.
28. Zhu, M.-F., W. Cao, S.-L. Chen, C.-P. Hong, and Y.A. Chang, *MODELING OF MICROSTRUCTURE AND MICROSEGREGATION IN SOLIDIFICATION OF MULTI-COMPONENT ALLOYS.* Journal Of Phase Equilibria and Diffusion, 2007. **28**(1): p. 130-138.

Table 1. Summary of evaluation results for the global optimization solver in PanEngine

Number of Variables	Function Evaluations	Optimal Value	Runtime(seconds)
1	446	3.17085e-031	0
2	814	4.16444e-013	0.015
3	1211	1.39536e-012	0.015
4	1344	3.47232e-012	0.015
5	1218	2.32691e-011	0.015
6	2008	2.01273e-011	0.015
7	2130	2.65424e-011	0.015
8	3423	4.1798e-011	0.016
9	2929	3.30411e-011	0.015
10	3555	3.62034e-011	0.016

Table 2. Benchmark results for PANDAT 7 and PANDAT 5

System	Calculation Type	$t(V7)$ **(sec)**	$t(V5)$ **(sec)**	$\frac{t(V7)}{t(V5)}$
148 Binaries	2D - Section	440	1686	3.83
NI625	0D - Point	1	8	8.0
IN718	1D - Line	12	87	7.25
Ni-Al	2D - Section	6.0	30	5.0
Ni-Al-Ru	2D - Section	12	47	3.92
Ni-Al-Pt	2D - Section	24	87	3.625
Ni-Al-Ir	Liquidus Projection	15	87	5.8
Nb-22Ti-2Hf-4Cr-3Al-16Si	Solidification Simulation - Scheil	20	50	2.5
Nb-22Ti-2Hf-4Cr-3Al-16Si	Solidification Simulation – Lever Rule	5	19	3.8

Note: $t(V7)$ denotes the time used by PANDAT 7 and $t(V5)$ is the time used by PANDAT 5.

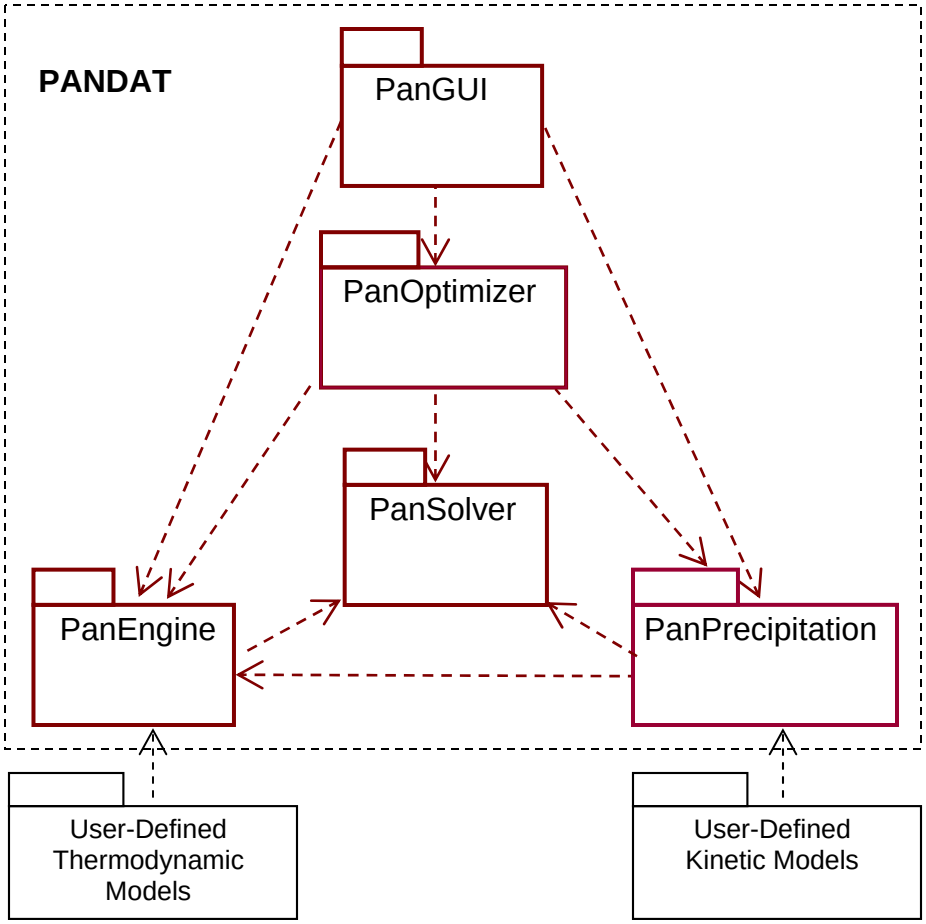

Figure 1. The top level module dependencies for PANDAT.

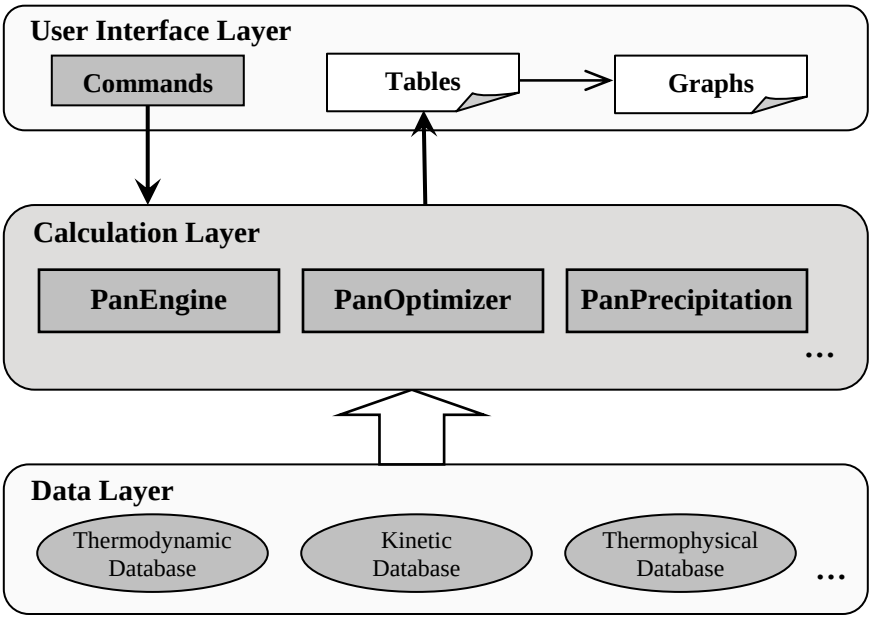

Figure 2. Software architecture of PANDAT.

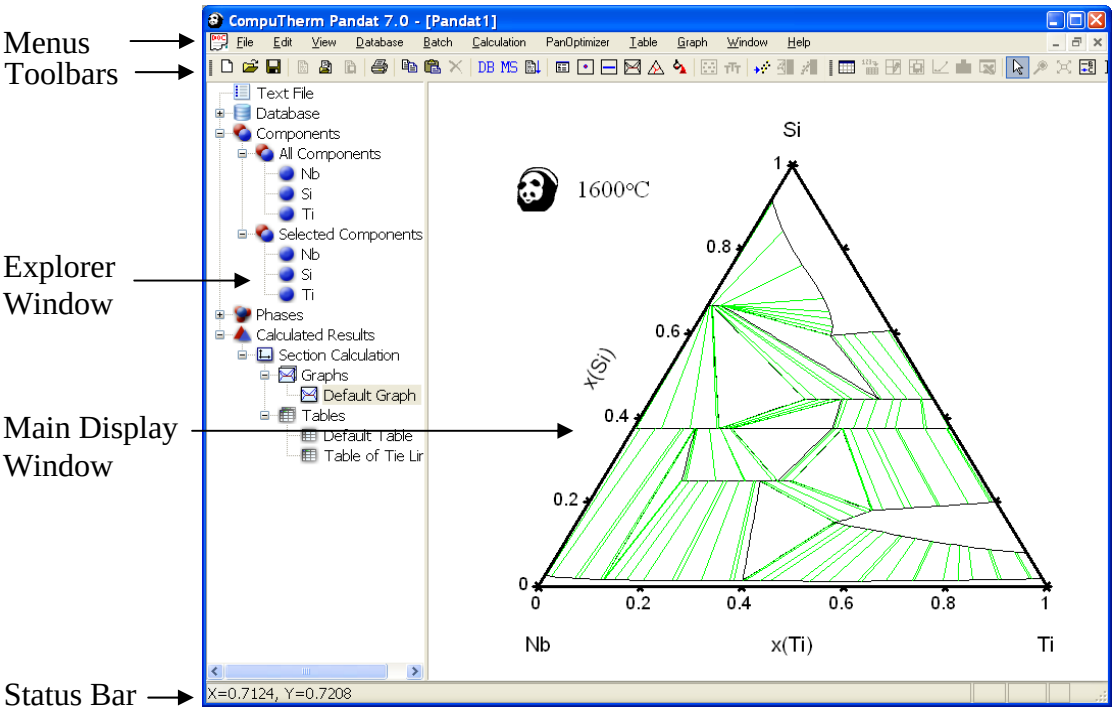

Figure 3. User Interface of PANDAT Workspace

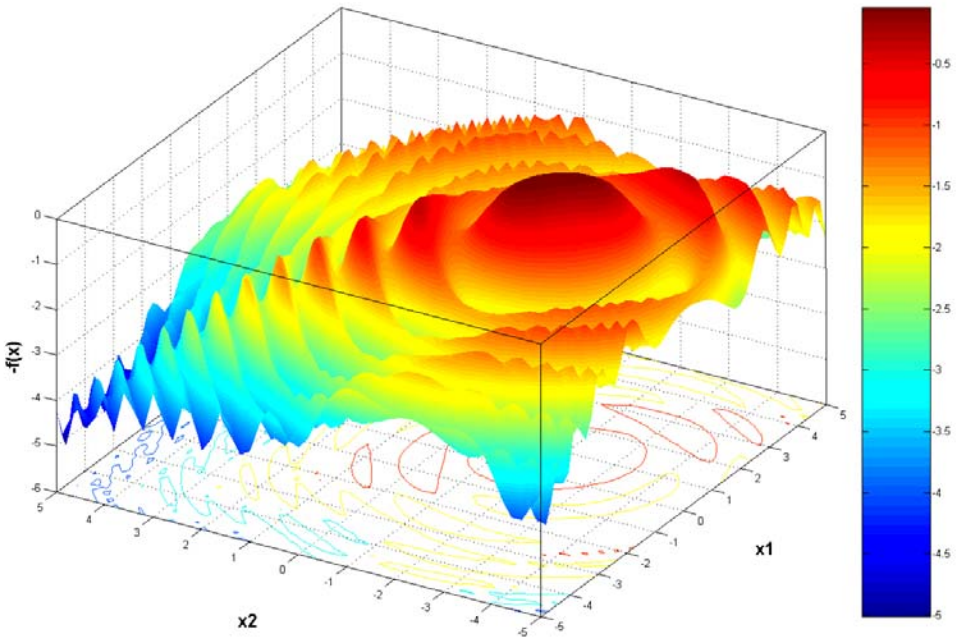

Figure 4. A randomly generated two-dimensional global optimization test function (Equation 4, n = 2).

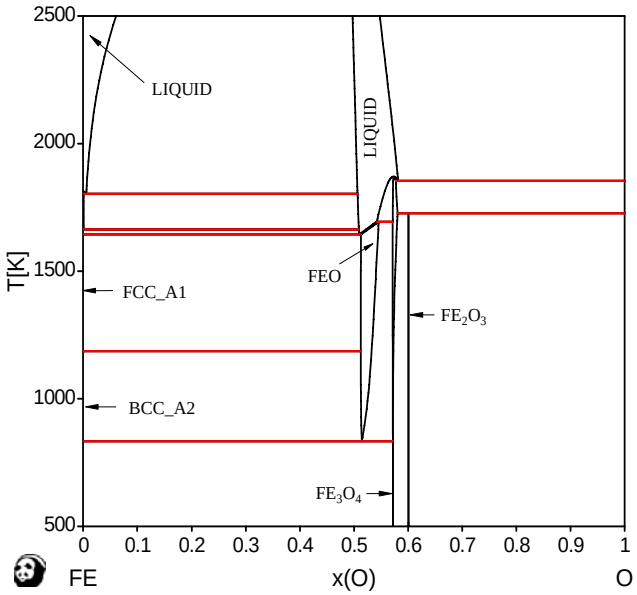

Figure 5. Calculated binary Fe-O phase diagram.

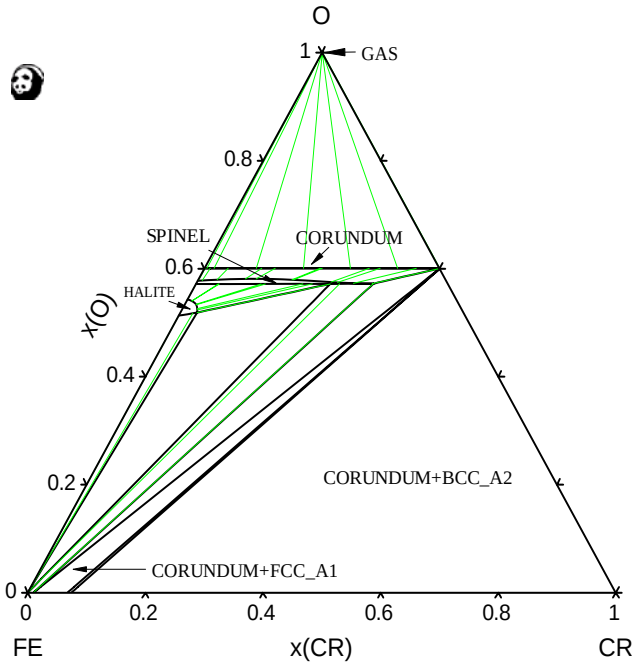

Figure 6. Calculated isothermal section of Fe-Cr-O system at 1573 K.

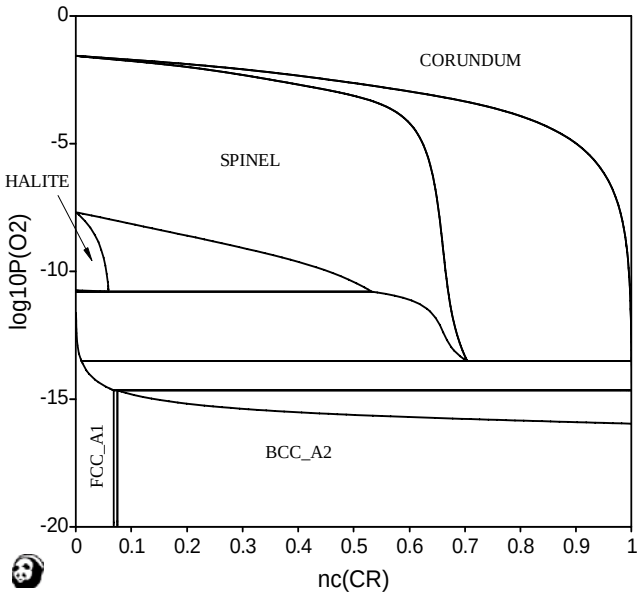

Figure 7. Calculated stability diagram of Fe-Cr-O system at 1573 K.

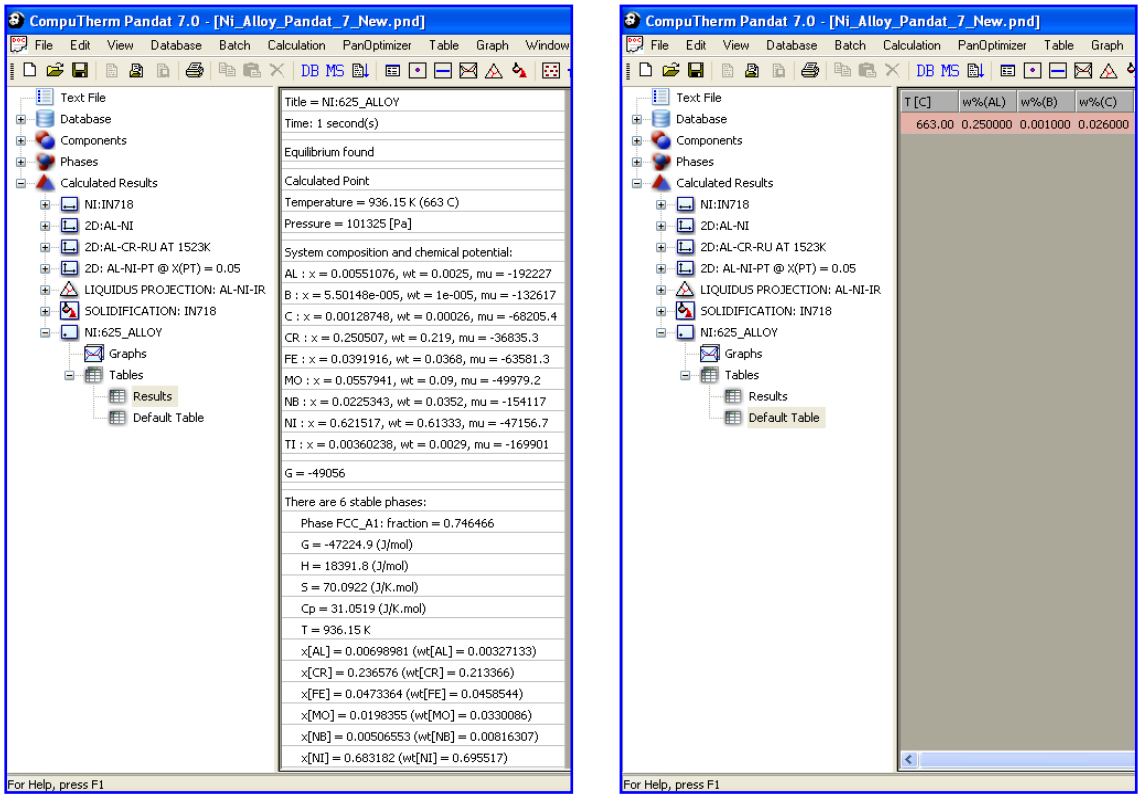

(a) **(b)**

Figure 8. PANDAT *point calculation* results of alloy 625

(a) in a list table and (b) in a grid table (customizable); an extended grid table is automatically generated by a PANDAT *point calculation.*

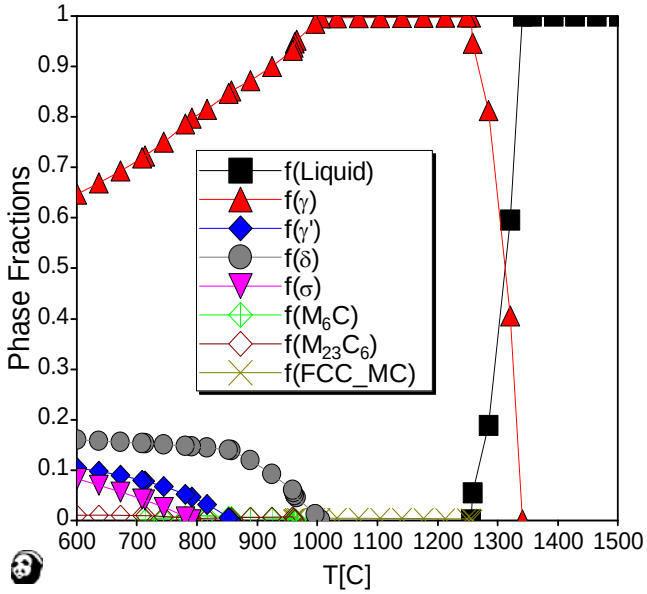

Figure 9. Line calculation results of alloy 718 from 1500°C to 600°C.

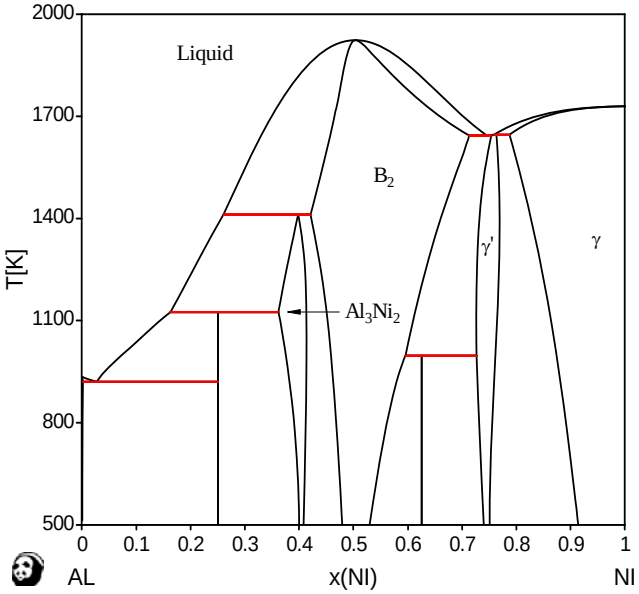

Figure 10. Calculated binary Ni-Al phase diagram.

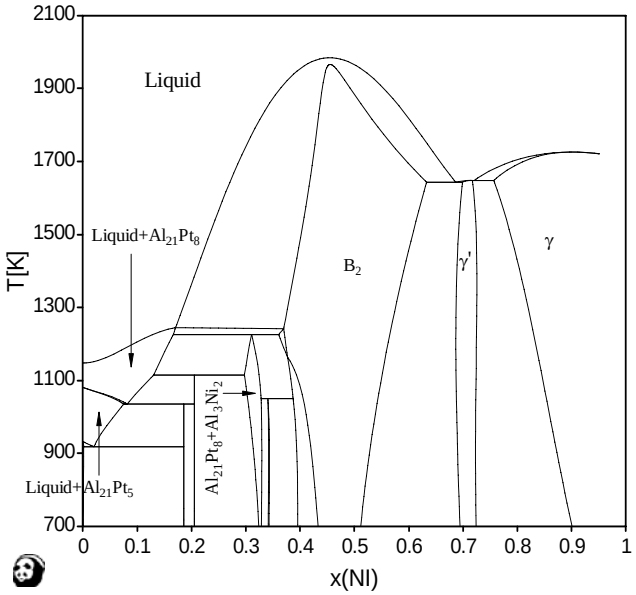

Figure 11. Calculated isopleth for Ni-Al-Pt system with the mole fraction of Pt being fixed at 0.05.

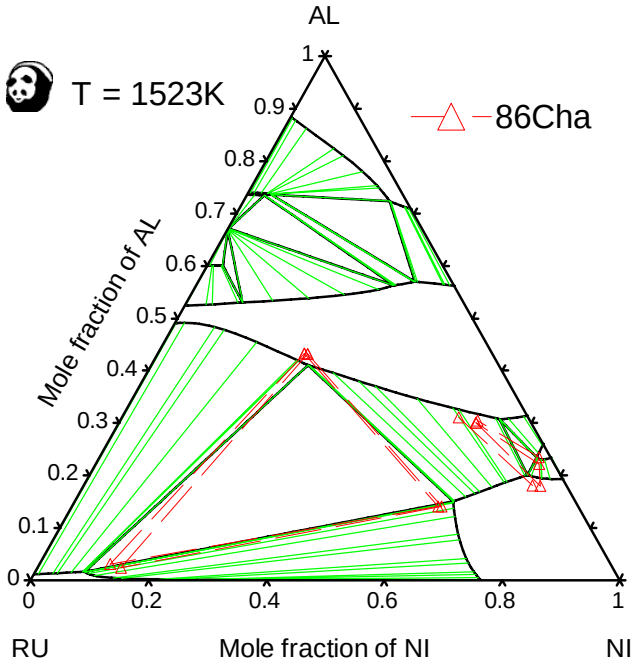

Figure 12. Calculated isothermal section for Ni-Al-Ru system at 1523K compared with the experimental data.

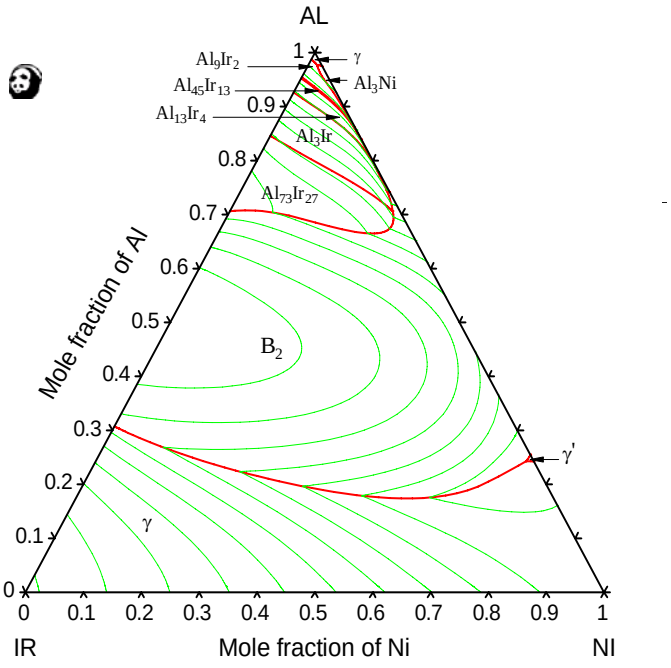

Figure 13. The liquidus projection for Ni-Al-Ir system.

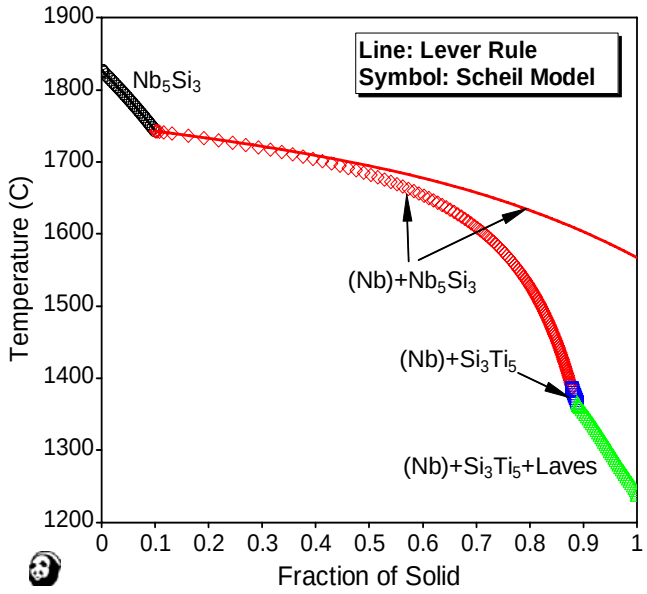

Figure 14. Calculated solidification paths for a niobium alloy (Nb-22Ti-2Hf-4Cr-3Al-16Si in at%) using PANDAT under Lever Rule and Scheil conditions.

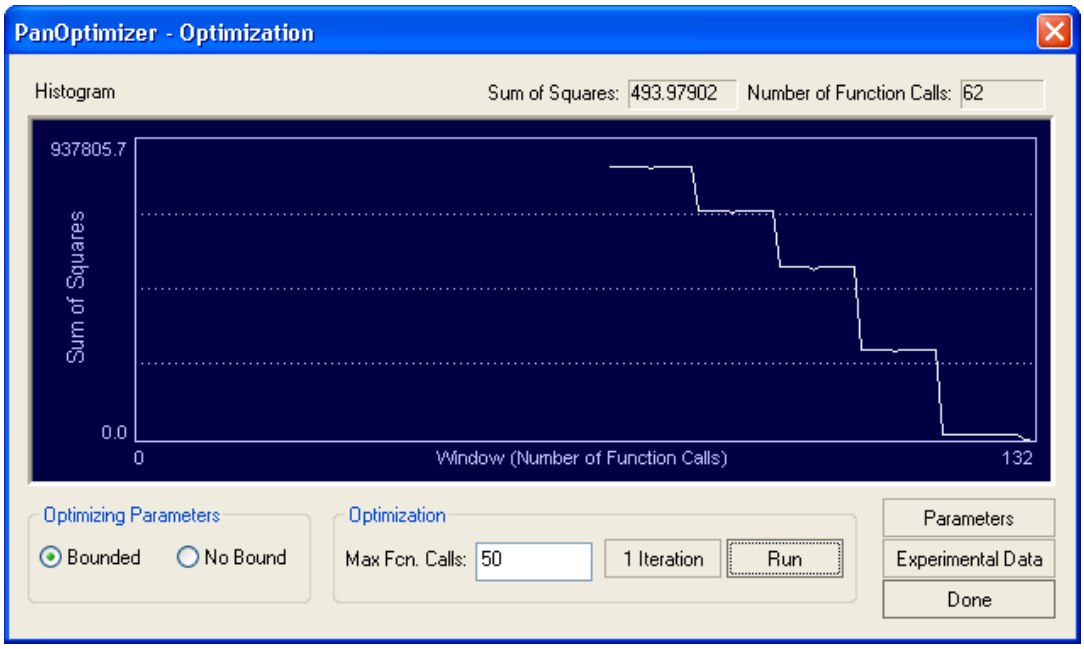

Figure 15. The control panel of PanOptimizer for normal optimization.

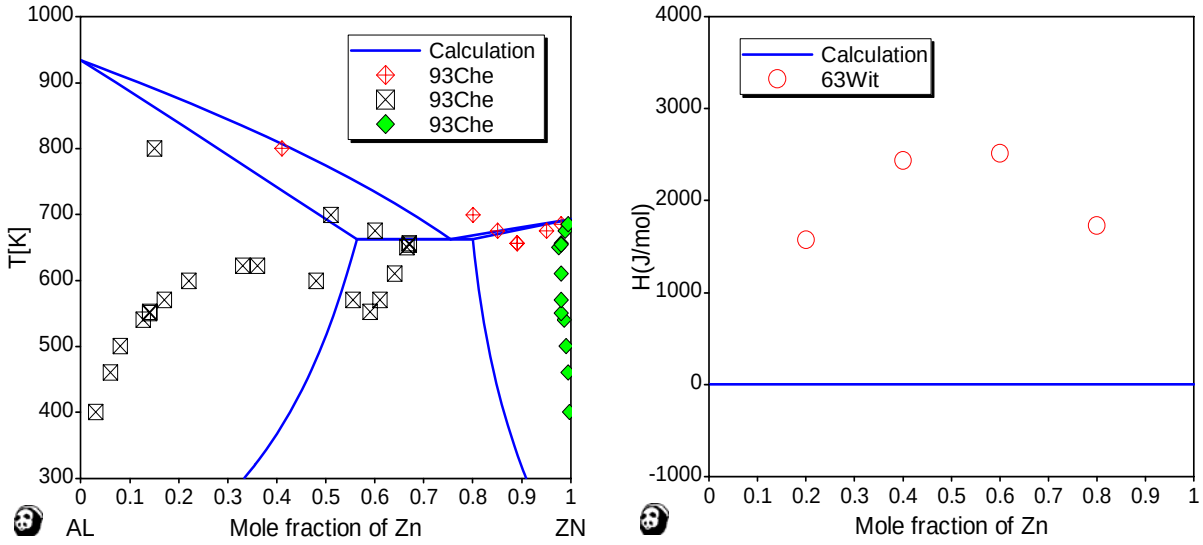

(a) **(b)**

Figure 16. (a) The phase diagram and (b) the enthalpy of the liquid phase of the binary Al-Zn system before the optimization.

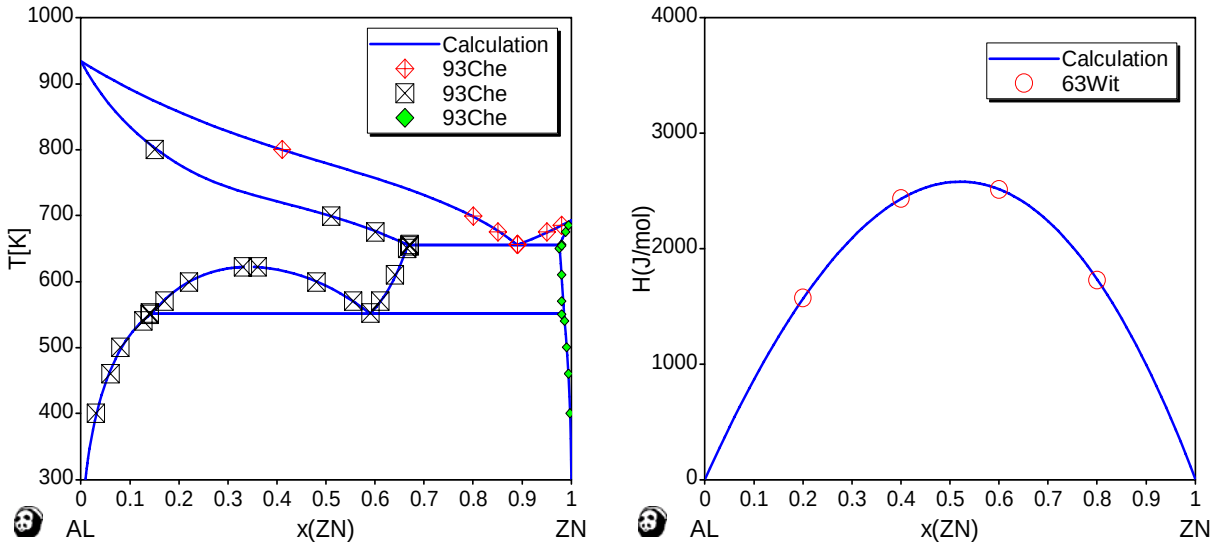

(a) **(b)**

Figure 17. (a) The phase diagram and (b) the enthalpy of the liquid phase of the binary Al-Zn system after the optimization.

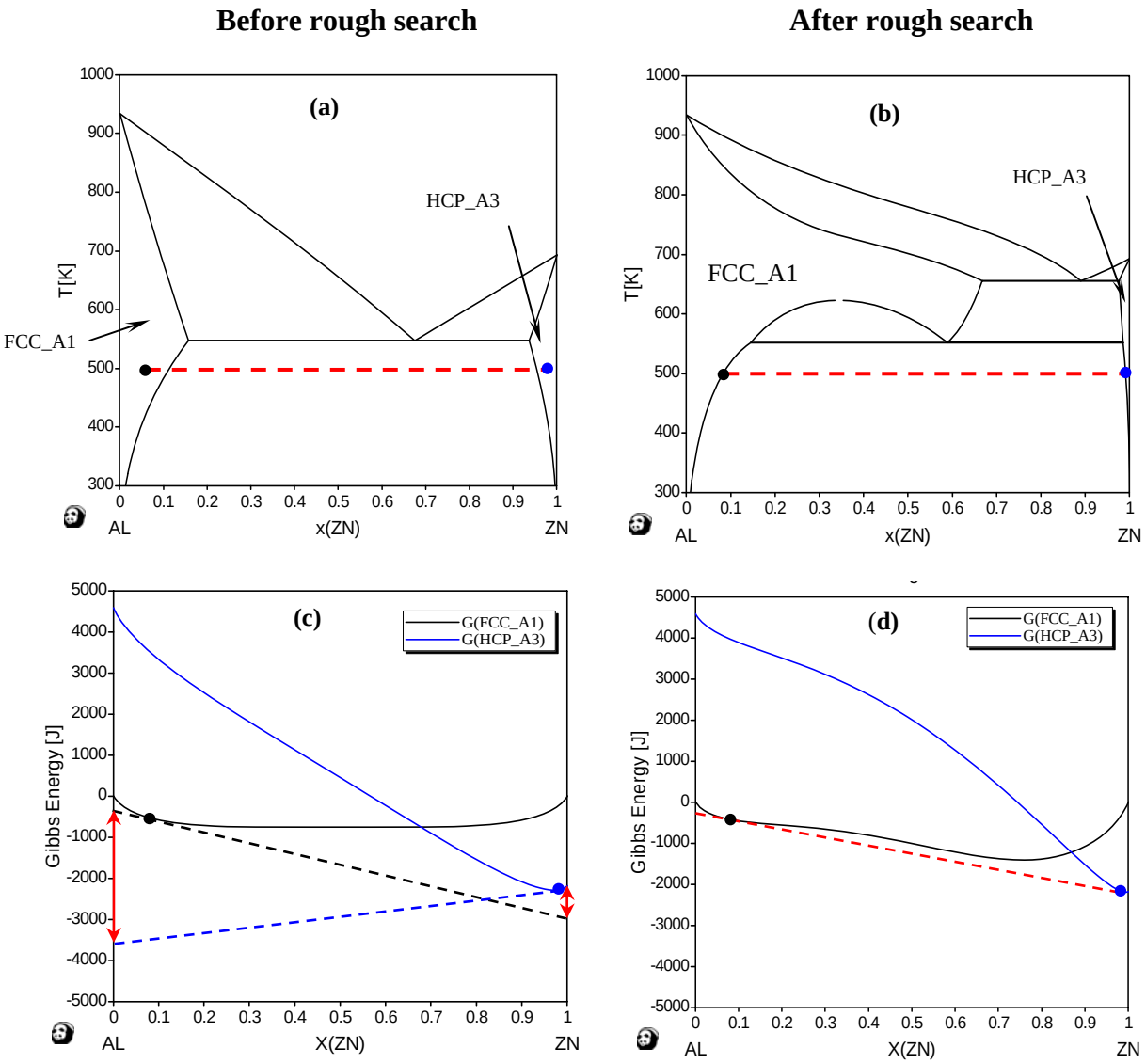

Figure 18. (a) Calculated Al-Zn phase diagram before the rough search; (b) Calculated Al-Zn phase diagram after the rough search; (c) Calculated Gibbs energy curves before the rough search; (d) Calculated Gibbs energy curves after the rough search;

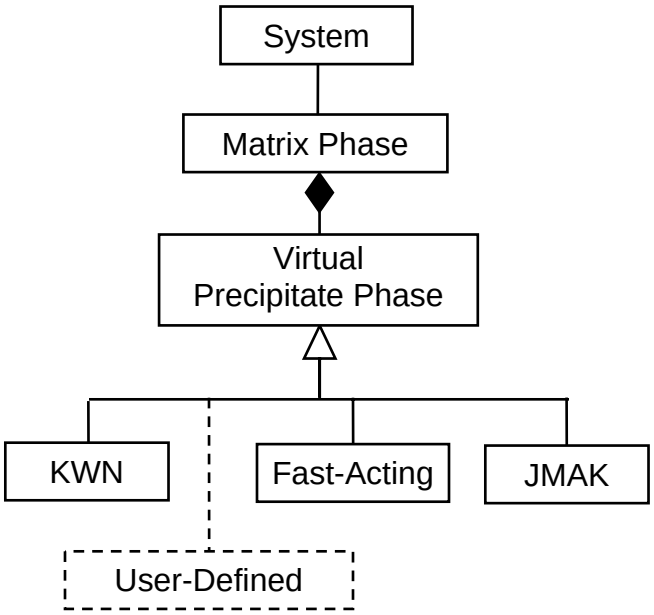

Figure 19. Date structure of system information in PanPrecipitation.

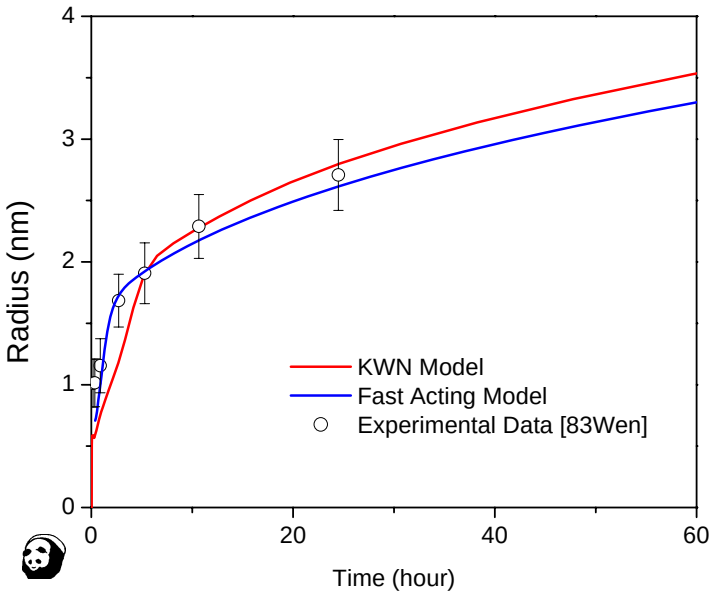

Figure 20. Predicted evolution of average γ' particle size with time compared with the experimental data.

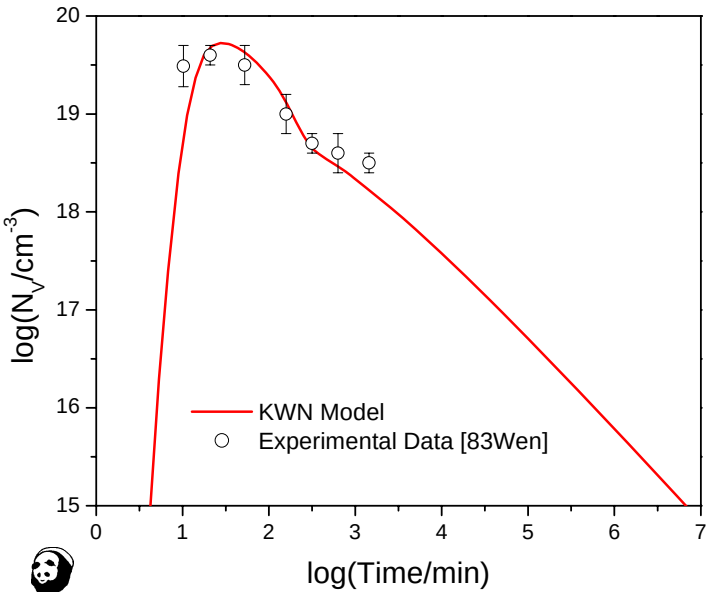

Figure 21. KWN-predicted evolution of γ' number density with time compared with the experimental data.

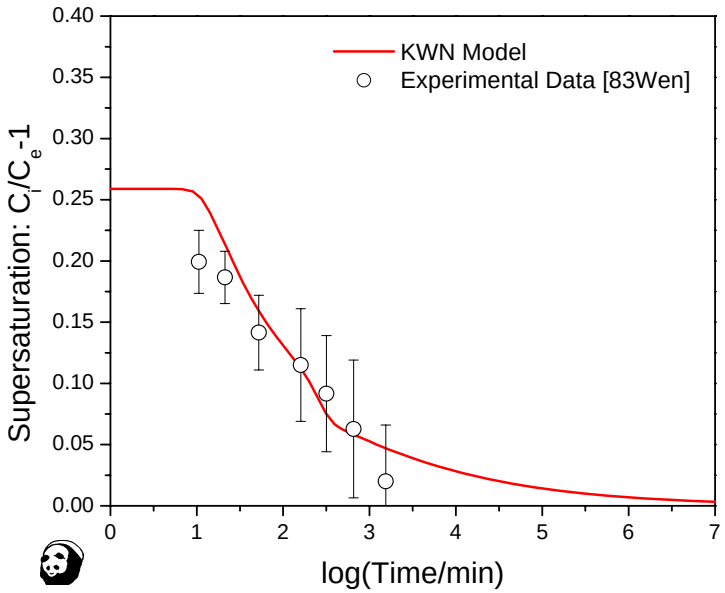

Figure 22. KWN-predicted evolution of supersaturation with time compared with the experimental data; C_i is the instantaneous matrix composition far away from the interface and C_e is the equilibrium matrix composition.

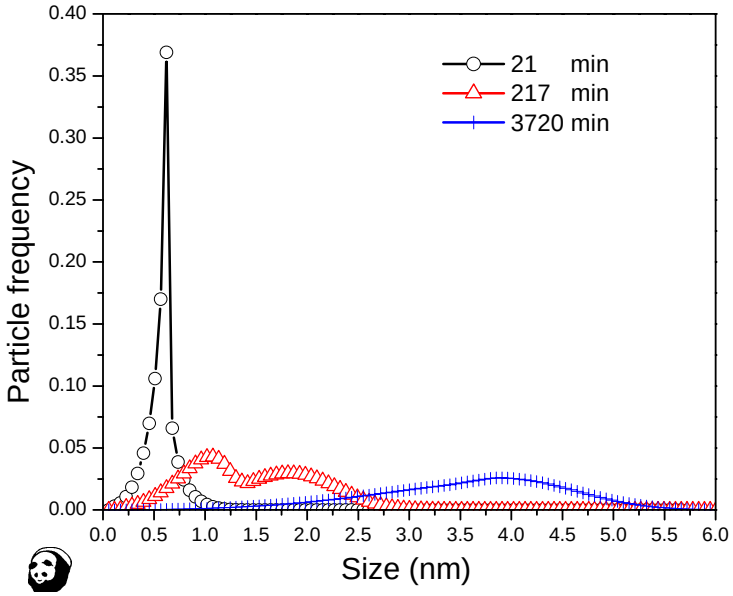

Figure 23. KWN-predicted particle size distributions for the γ' particles at t = 21, 217 and 3720 min.

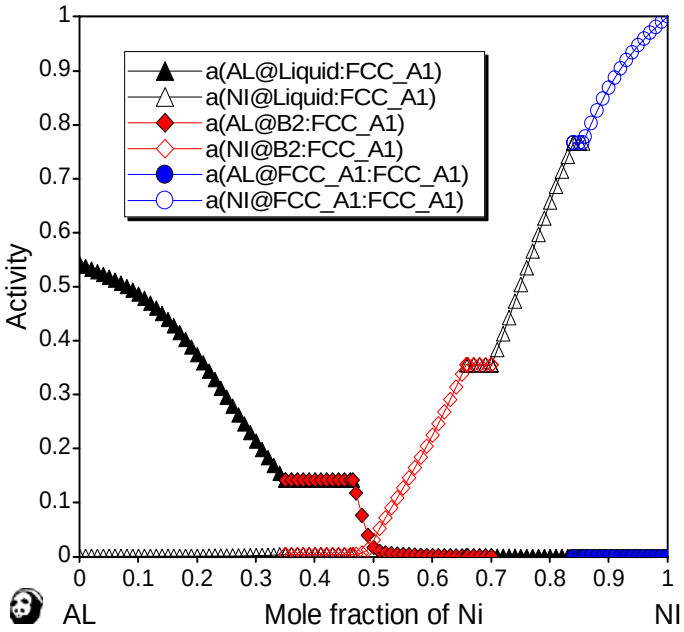

Figure 24. Calculated activities of Liquid, B2 and FCC_A1 phases as a function of mole fraction of Ni in Ni-Al at 1700K.

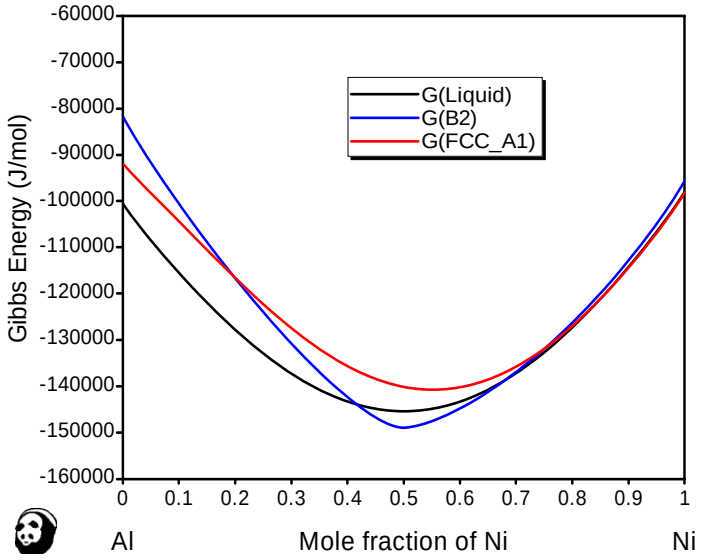

Figure 25. Calculated Gibbs energies of Liquid, B2 and FCC_A1 phases as a function of mole fraction of Ni in Ni-Al at 1700K.

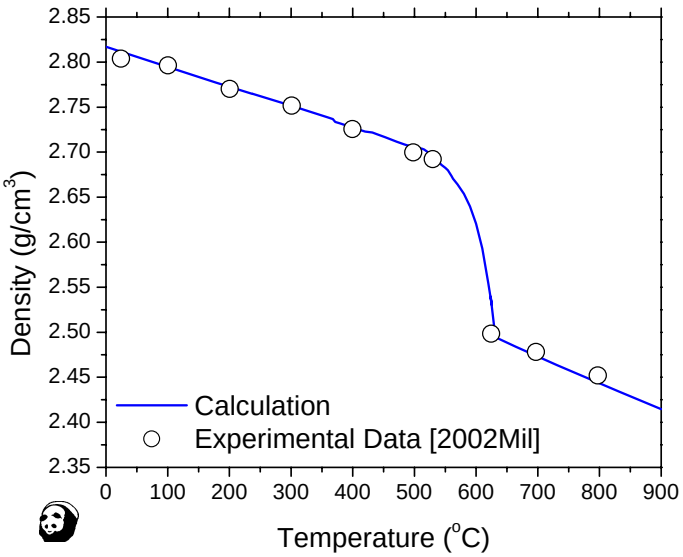

Figure 26. Calculated density of alloy Al-7075-T6 as a function of temperature compared with the experimental data.

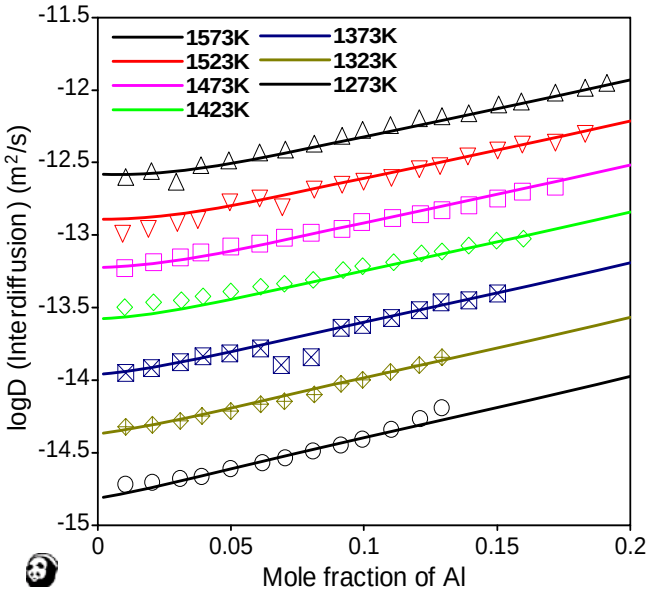

Figure 27. Calculated inter-diffusivity vs. composition at different temperatures for the binary Ni-Al system. Symbols in the figure denote the experimental data.

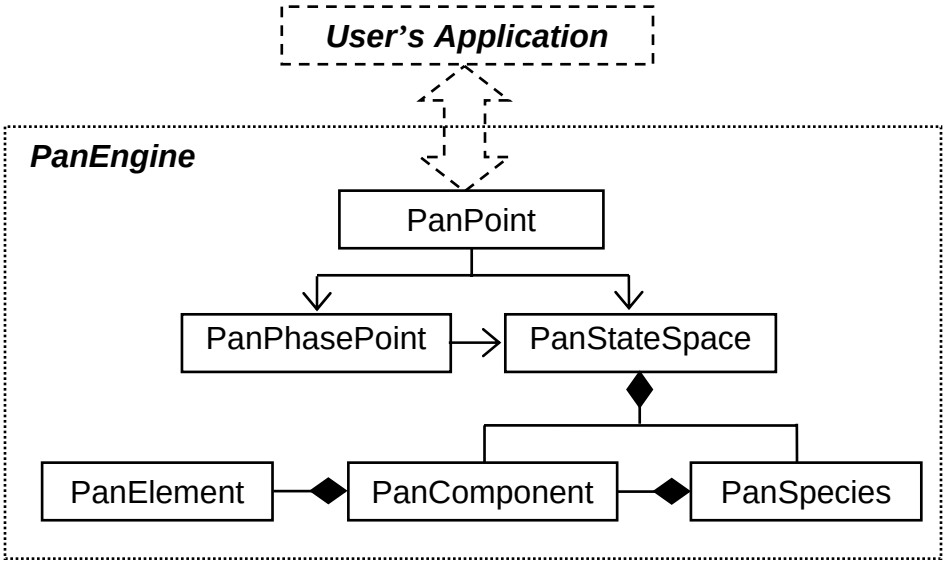

Figure 28. Data structure of system information for integration with PanEngine.

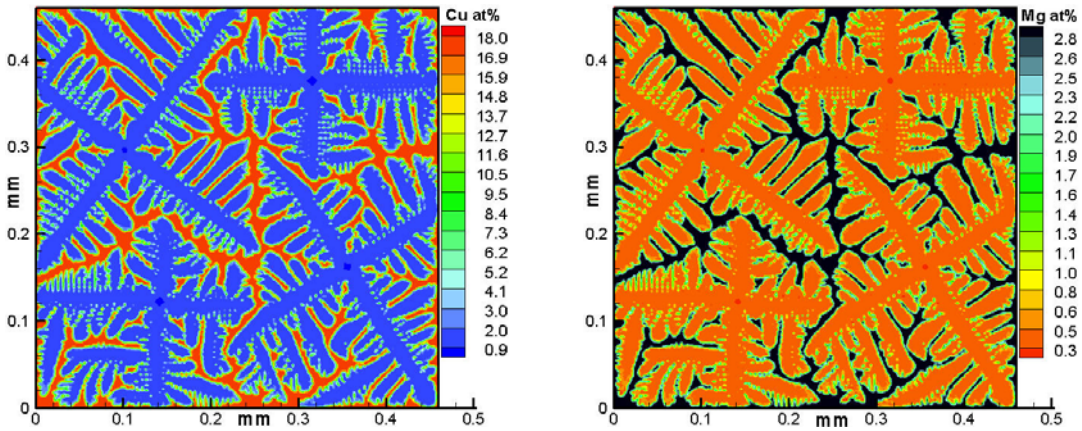

Figure 29. Simulated equiaxed dendrite morphology and solute fields of (a) Cu, and (b) Mg for an Al-15 wt% Cu-1 wt% Mg alloy solidified with 10 K/s.

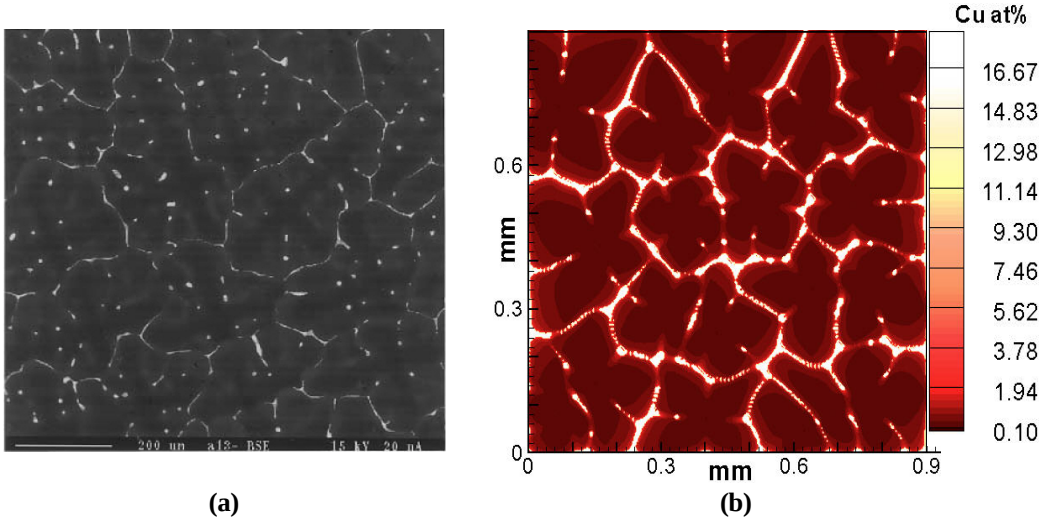

Figure 30. Dendrite morphology of an Al-3.9 wt% Cu-0.9 wt% Mg alloy solidified with 0.78 K/s: (a) experiment, and (b) simulation.